objectives: (1) developing an 8 degrees of freedom (DOFs) powered anthropomorphic exoskeleton for the arm, including grasping/releasing; (2) developing control algorithms that will fuse information from multiple sensors and will guarantee stable exoskeleton operation; and (3) evaluating the overall performance of the integrated system using standardized arm/hand function tests. These goals and objectives will be pursued using several experimental protocols aimed at developing the controllers and evaluating the exoskeleton performance. The proposed experimental protocol includes only healthy subjects as the first step in a long-term goal aimed at evaluating the exoskeleton performance with disabled subjects suffering from various neurological disabilities, such as stroke, spinal cord injury, muscular dystrophies, and other neurodegenerative disorders.

The development of this series of upper limb rehabilitation robotic exoskeleton systems in the Bionics Lab (University of Washington, University of California Santa Cruz, and University of California Los Angeles) integrates hardware, firmware, and software that includes human in the loop. This chapter illustrates the process of developing these four generations of upper limb exoskeletons: EXO-UL1 (myosignal-based, single-arm), EXO-UL3 (myosignal-based, single-arm), EXO-UL7 (force/torque-based, dual-arm), and EXO-UL8 (force/torque-based, dual-arm), as well as some ongoing research work.

5.2 EXOSKELETON SYSTEMS

5.2.1 PROTOTYPE 1 (EXO-UL1)

As the beginning of this serial research on rehabilitative robotic exoskeletons, the first exoskeleton mechanism consisted of a two-link, two-joint device corresponding to the upper and the lower arm and to the shoulder and elbow joints of the human body [4–6].

Shown in Fig. 5.1, the system included a weight plate (external load) that can be attached to the tip of the exoskeleton forearm link. The mechanism was fixed to the wall and positioned parallel to the sagittal plane of the operator. The human/exoskeleton mechanical interface included the upper arm bracelet, located at the upper arm link, and a handle grasped by the operator. This two-joint mechanism was used as a 1-DOF system by fixing the system shoulder joint at specific angles in the range of 0–180 degrees. The elbow joint was free to move in an angle range of 0–145 degrees, and included built-in mechanical constraints which kept the exoskeleton joint angle within the average human anthropometric boundaries. Since the human arm and the exoskeleton were mechanically linked the movements of the forearms of both the human and the exoskeleton were identical.

The basic purpose of the exoskeleton system as an assistance device is to amplify the moment generated by the human muscles relative to the elbow joint, while manipulating loads. The exoskeleton's elbow joint was powered by a DC servo motor (ESCAP-35NT2R82) with a stall torque of 360 mNm equipped with a planetary gearbox (ESCAP-R40) with a gear ratio of 1:193 and a maximal output torque of 40 Nm. An optical incremental shaft encoder (HP HEDS 5500) with 500 lines was attached to the motor shaft. Due to the encoder location and the high gear ratio, the practical encoder's resolution for measuring the joint angle was 0.0036 degrees. This setup incorporated a DC motor with the highest torque-to-weight ratio that was available on the commercial market at that time with power consumption that could be provided by a battery. A high energy density of the power supply and an actuator with a high torque-to-weight ratio are two key features of the

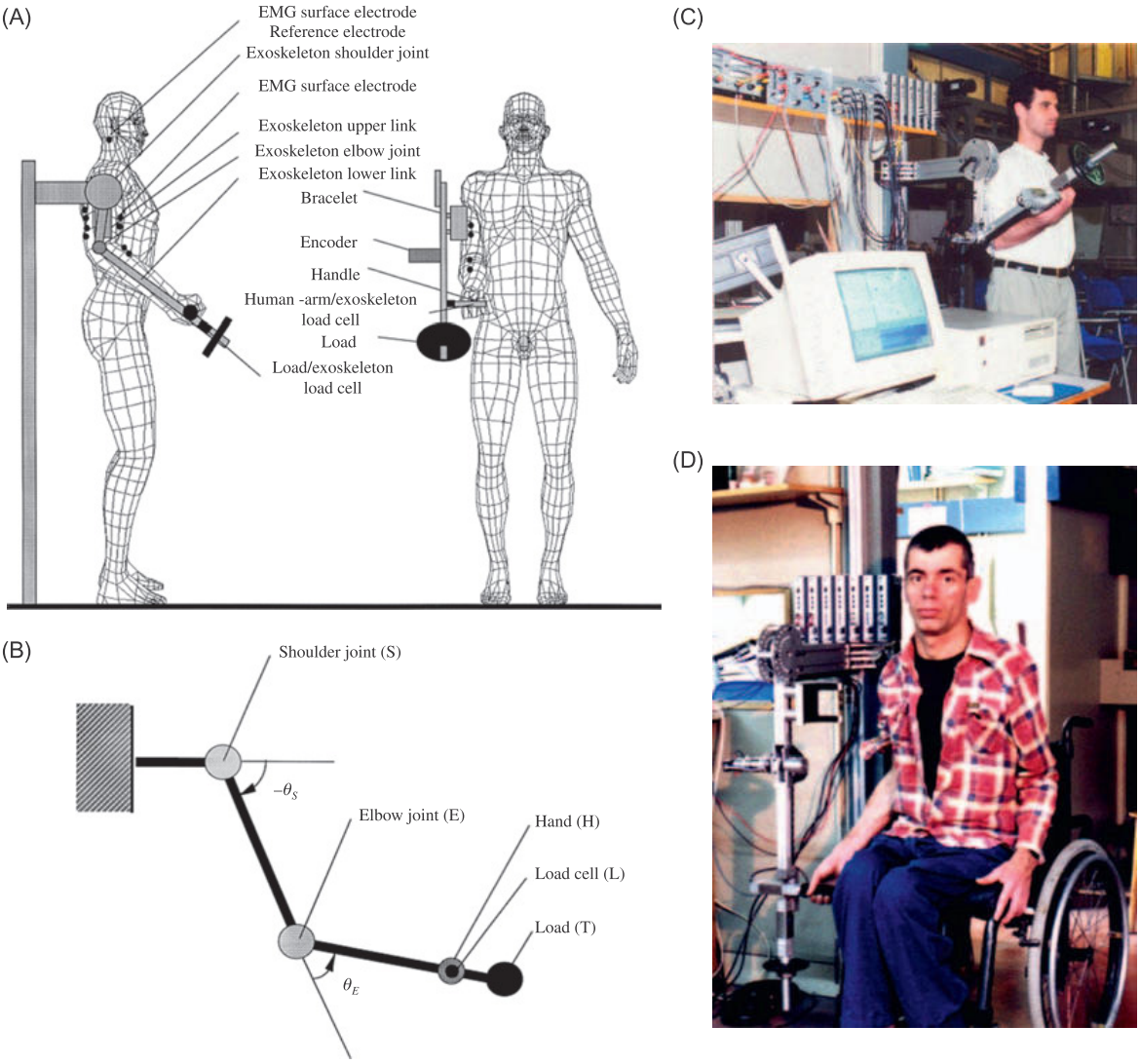

FIGURE 5.1

(A) Frontal and lateral view of the experimental setup: the exoskeleton and human operator. (B) Schema of the two-link, two-joint exoskeleton. (C) A human operator is using the exoskeleton device. (D) The EXO-UL1 system tested with a disabled person suffering from Tay-Sachs [7].

exoskeleton system as a self-contained mobile medical assistance device for the disabled community. Limits imposed by the technologies at that time on these two key components along with design requirements for developing a compact system with a potential of serving as a medical assistance device for disabled person restricted the payload to 5 kg. However, this biomedical-oriented design does not restrict the generality of the exoskeleton concept or its operational algorithms. Using other actuation systems, like a hydraulic system, increases the load capacity substantially.

The exoskeleton forearm was extended by a rod with a special connector for attaching disk-type weights (external load). Two force sensors (TEDEA 1040) were mounted at the interfaces between the exoskeleton and the tip carrying the external load and between the exoskeleton and the human hand. The first load cell, inserted between the rod holding the external load and the exoskeleton forearm link, measured the actual shear force, normal to the forearm axis, applied by the external load. The second load cell was installed between the handle grasped by the human hand and the forearm link of the exoskeleton. This load cell measured the shear force applied by the operator to the handle. Multiplying the sensors' measurements by the corresponding moment arms indicated the moments applied by the weights and by the human hand relative to the elbow joint.

One of the primary innovative ideas of the research was to set the Human Machine Interface (HMI) at the neuromuscular level of the human physiological hierarchy using the body's own neural command signals as one of the primary command signals of the exoskeleton. These signals will be in the form of processed surface electromyography (sEMG) signals, detected by surface electrodes placed on the operator's skin. The originally proposed HMI takes advantage of the electrochemical−mechanical delay, which inherently exists in the musculoskeletal system, between the time when the neural system activates the muscular system and the time when the muscles generate moments around the joints. The myoprocessor is a model of the human muscle running in real-time and in parallel to the physiological muscle. During the electrochemical−mechanical time delay, the system will gather information regarding the physiological muscle's neural activation level based on processed sEMG signals, the joint position, and angular velocity, and will predict, using the myoprocessor, the force that will be generated by the muscle before physiological contraction occurs. By the time the human muscles contract, the exoskeleton will move with the human in a synergistic fashion, allowing natural control of the exoskeleton as an extension of the operator's body.

Surface EMG electrodes (8 mm Ag-AgCl BIOPAC—EL208S) were attached to the subject's skin by adhesive disks for measuring the EMG signal of the biceps brachii and triceps brachii medial-head muscles. The signals were gained by EMG amplifiers (BIOPAC—EMG100A) using a gain factor in the range of 2000−5000 (depending on the subject). The EMG signals and the load cell signal were acquired by an A/D convector (Scientific Solution Lab Master 12-bit internal PC card) with a 1 kHz sampling rate, whereas the encoder signals were counted by custom-made hardware. The entire data set was recorded simultaneously and stored, for later off-line analysis and simulation.

A special real-time software, for operating the system, was written in C and run on a PC-based platform. The software was composed of three main modules. The first module dealt with the hardware/software interface. It controlled the interaction between the PC and the external motor driver and the sensors, through a D/A and an A/D card. The second module included the automatic code generated by the MATLAB−Simulink Real-Time toolbox. The third module was the user interface module which allowed setting of various run time operational parameters. All the modules were compiled and linked for generating an efficient real-time software.

5.2.2 PROTOTYPE 2 (EXO-UL3)

The second exoskeleton mechanism, shown in Fig. 5.2 [7], consisted of a three-link, two-joint device corresponding to the upper and the lower arm and the shoulder and elbow joints of the

FIGURE 5.2

EXO-UL3 Robotic Exoskeleton System.

human body. The hardware is similar to the first mechanism except that it was used as a 2-DOF system: the elbow and the shoulder joints were free to move in their anatomical range of motion.

Four force sensors (TEDEA 1040) were mounted at the interfaces between the exoskeleton and the operator: one at the tip carrying the external load, two between the exoskeleton and the human hand, and one at the interface between the upper arm and the exoskeleton. Like the first generation, the first load cell, inserted between the rod holding the external load and the exoskeleton forearm link, measured the actual shear force, normal to the forearm axis, applied by the external load. The other load cells were installed between the handle grasped by the human hand and the forearm link of the exoskeleton and between the upper arm bracelet and the exoskeleton upper link. These load cells measured the shear forces applied by the operator to the mechanism. Multiplying the sensors' measurements by the corresponding moment arms indicated the moments applied by the weights and by the human arm relative to the elbow and the shoulder joints.

Expanding the DOFs the mechanism could facilitate from three to seven, and eventually eight, took the research team several years—a leap to EXO-UL7.

5.2.3 PROTOTYPE 3 (EXO-UL7)

Note: this generation of anthropometric 7-DOF powered exoskeleton system was once termed as "Cable-Actuated Dexterous Exoskeleton for Neuro-rehabilitation" (CADEN-7) [8], but soon afterward the authors decided to uniform its name under the "EXO-UL" series [9].

Based on the human arm kinematics and dynamics during activities of daily living [10], for the first time in this exoskeleton system series, the EXO-UL7 shown in Fig. 5.3 covers all seven major

FIGURE 5.3

EXO-UL7 Robotic Exoskeleton System.

DOFs of the human upper limb including shoulder extension/flexion, shoulder adduction/abduction, shoulder internal/external rotation, elbow extension/flexion, forearm pronation/supination, wrist extension/flexion, and wrist radial/ulnar deviation [7,11–13]. It also contains two arms and enables more training protocols that will be further discussed in the EXO-UL8 section.

At first the controller was based on the sEMG [14,15], but due to the cumbersomeness of setting up an sEMG measuring system in practical rehabilitation applications, the research shifted to using force/torque sensors only. For details of gravity compensation implementation please refer to Ref. [16], of PID control [17,18], and of neural PID control [19].

For more details on the design of this generation of exoskeleton system, readers are encouraged to read the PhD dissertation from Joel C. Perry [12]; for the general control part, readers are encouraged to read the PhD dissertations from Miller [20] and Kim [21].

5.2.4 PROTOTYPE 4 (EXO-UL8)

The strength and maximum power output of EXO-UL7 were limited by the cable-driven mechanism. Therefore the authors modified the design to a motor-gear actuated one. Some of the recent progress in the EXO-UL8 (Fig. 5.4) was covered in Refs. [22–25]. Here the authors try to provide an overview in a more systematic way.

5.2.4.1 System architecture

The dual exoskeleton system includes two major components: (1) hardware—robotic mechanism, actuation, sensing and electronics; and (2) software—control architecture, and virtual reality (VR) environment. The human is physically attached to the exoskeleton system. Contact forces are

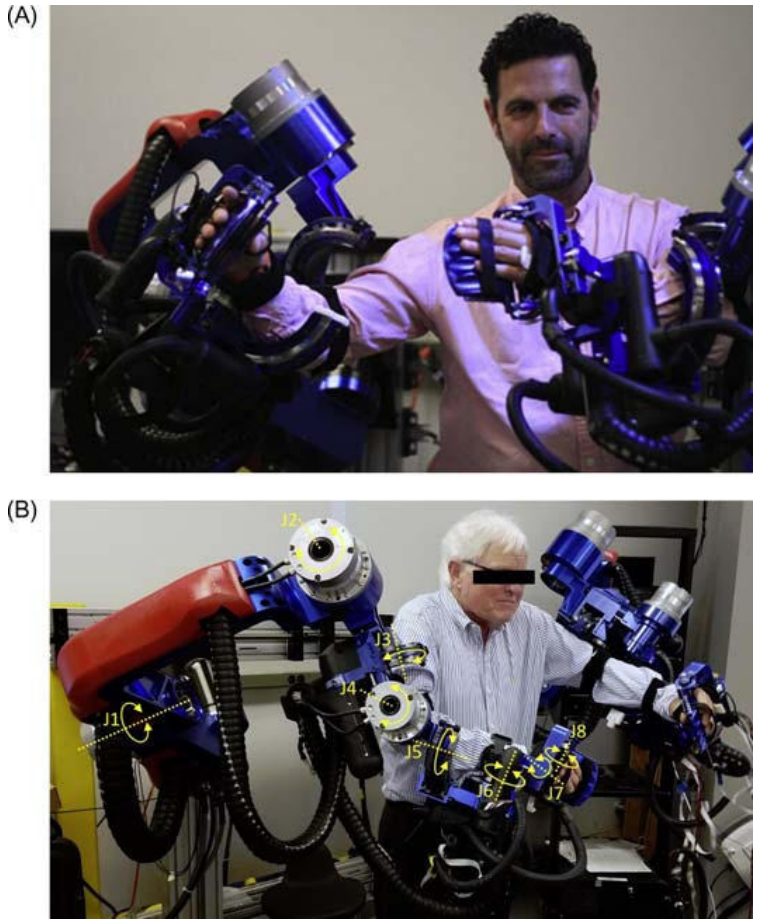

FIGURE 5.4

(A) One of the authors is operating the EXO-UL8 Robotic Exoskeleton System; (B) A poststroke patient is operating the EXO-UL8 Robotic Exoskeleton System.

measured by force sensors placed between the braces (upper arm, forearm, palm, and fingers) and the exoskeleton structure. Joint angles are measured by encoders located on the shafts of the joints. These two types of signals are converted via the A/D and a counter, respectively, by the real-time PC. Using an array of algorithms, encoded into the real-time PC, joint torque commands are generated and converted via the D/C by the real-time PC as inputs to the servo amplifiers. The servo amplifiers operated in a current mode control the actuation system which in turn results in its movement along with the application of the force fields. Feedback control signals are generated based on modes of operation: unilateral or bilateral. Joint angles are also sent via UDP protocol to the VR PC. The VR scene including a representation of the operator's arm along with all the virtual objects is rendered and displayed to the operator on a screen. The physics engine renders the haptic force fields information that is applied to the operator's arms by the exoskeleton system.

5.2.4.2 Mechanism, actuation, and sensing

The fourth generation (EXO-UL8) of a dual anthropometric arm exoskeleton system was designed and fabricated based on lessons learned for the extensive use of the system in the past in both a lab and clinical settings with stroke patients.

- *Mechanism (Adjustable Links Length)*—The mechanism includes a total of 8 DOF (3 DOFs for the shoulder joint, 2 DOFs for the elbow joint, 2 DOFs for the wrist joint, and 1 DOF of the hand). The entire two exoskeleton arms are attached to a portable frame and a chair that allows changing the height and distance (shoulder span) of the two arms. The length of the upper arm and the forearm are adjustable allowing the therapist to fit these two dimensions to various arm lengths in the range of the 5−95 percentile of the populations' anthropometric data. The rotation axes of the exoskeleton system intersect at the centers of the anatomical joints in a way that eliminates any potential joint dislocation. The mechanical joint includes hard joint limits that match the range of motion of the anatomical joint. The first three shoulder joints are oriented with respect to the patient in such a way that they position the singular configuration of the shoulder joint out of the human arm workspace. Furthermore, a single passive DOF was added to the wrist in addition to the existing two actuated DOFs in order to avoid any internal joint torque. The anthropometric design of the exoskeleton allows the user to reach 95% of the workspace accessible to the healthy operator. The human operator is physically attached to the exoskeleton arm and interacts with the system through five physical interfaces. Three braces are attached to the upper arm, the forearm, and the palm. An additional two contact surfaces form the claw-type hand interface.
- *Actuation*—This generation of the system uses actuators that are directly connected to each of the 8 DOFs of the system. Pancake coil brushless DC actuators with harmonic drive are used for the large joints (shoulder and elbow), and small form factor Maxon DC brushed motors with multistage gearboxes are used for the smaller joints (wrist and hand). The selected actuators have the largest torque-to-weight ratio available in an off-the-shelf actuation system at the time it was developed.
- *Hands*—The new generation of the system includes two types of hands: (1) claw-type single DOF hand; and (2) three-finger multi-DOF hand (under development [26]). The exoskeleton arm includes a universal interface at the proximal end of the arm allowing the mounting and interchanging of the two hands. The claw-type single DOF hand separates the fingers into two groups including the thumb and the rest of the fingers. The hand with its two supporting surfaces is rotated with a single actuated axis allowing a claw-type grasp. The three fingers multi-DOF exoskeleton type hand lumps the fingers into three groups: (1) the thumb; (2) the index; and (3) the middle finger, the ring, and the pinky fingers. Lumping the five fingers of the hand into three groups and a special alignment of the joints of the hand interface allow for comfortable manipulations of the fingers throughout the entire common workspace of each group of fingers.
- *Sensing*—There are two types of sensors embedded into the exoskeleton: (1) position sensors; and (2) force torque sensors. Absolute encoders are mounted to the back shaft of all the actuators for measuring the absolute joint angle of every DOF. The human operator is physically attached to the exoskeleton arm and interacts with the system through three physical interfaces of the arm and two to three interfaces at the hand depending on the hand

configuration. Three braces are attached to the upper arm, the forearm, and the palm. An additional two contact surfaces of the claw-type hand interface and three contact interfaces for the three fingers hand transmit forces between the exoskeleton hand and the operator's fingers. Force sensors embedded into the braces and the supporting surfaces of the fingers enable the operator to control the arm and the hand using an admittance controller.

5.3 RELATED RESEARCH

5.3.1 CONTROL ALGORITHMS

Control algorithms on the series of exoskeleton systems have been improved over the years, from sEMG-based to force/torque-based. Adding strength to the mechanism from cable-driven to motor-gear also brings complexity to the control system, making it unruly and easily unstable.

Originally the admittance controller was used for high-level HMI intention detection: forces and torques were fed in and position/velocity commands were generated, and the strategy was compared in joint space and task space on EXO-UL7 [27]. Later on, the performances of hyperparameter-based and Kalman Filter–based admittance controllers were compared on EXO-UL8 [25].

For more details on the most recent progress, readers are encouraged to refer to Ref. [25].

5.3.2 REDUNDANCY RESOLUTION

Both the mechanisms of human upper limb [28] and the EXO-UL7 or EXO-UL8 exoskeleton [29] are redundant in 3D Cartesian space [30]. A variety of studies thus have been done on this topic: a viscoelastic model for redundancy resolution of the human arm was built in [31], the redundancy resolution was incorporated into the task space admittance control algorithm [32] to reduce energy exchange, and it was further studied based on kinematic and dynamic constraints [33].

Depending on the task type, the redundancy resolution of the human upper limb has been investigated for point/reach tasks [34–37], reach-to-grasp tasks [38,39], and reach tasks with gravitational loads [40]. The understanding of redundancy resolution was applied to predict human arm posture [41], as well as the EXO-UL7 exoskeleton configuration [42].

A better understanding of redundancy resolution is beneficial for the design and development of compliant control, force fields (for compensation correction), as well as a resistance training controller. For more details, please refer to the book [43] and the PhD dissertation from Zhi Jane Li [44].

5.3.3 SYNERGY ANALYSIS

While it is common for poststroke patients to have abnormal synergies, the symptom is not well quantified—a common way to access the multijoint coordination/independence is Fugl-Meyer Assessment (FMA) [45]. However, to the authors' understanding, the quantification of FMA is not fine enough for differentiating patients with similar scores. The synergetic effects between joints have been investigated on, in different scenarios, modeling [46,47]; rhythmic effects [48];

stroke-induced synergistic phase shifting [49], etc. For details on the human movement synergies, the readers are encouraged to read the MS thesis from Aimen Hamid Al-Refai [50], and the PhD dissertation from Matt Simkins [51].

5.3.4 DUAL-ARM TRAINING

Compared with unilateral training, dual-arm training may have potential benefits [52]. The dual-arm exoskeleton, which uses interarm teleoperation, has the capability of enabling different dual-arm training modes, including mirror-image symmetric bilateral training mode, and asymmetric (asynchronous) bilateral training mode. For bilateral symmetric training and related analysis, please refer to Refs. [53–57]; for asymmetric dual-arm training, please refer to Ref. [24] for more details. Research on arm motion similarity has also been reported [58,59].

5.3.5 VIRTUAL REALITY

As an accompanying module, VR has been developed along with the R&D of the exoskeleton [60,61]. The newest version of the VR module could be used with an exoskeleton or head-mounted devices (e.g., Oculus Rift). The research has been filed for a patent (No. 62/732,736).

5.4 SUMMARY

This chapter reviews all four generations of the upper limb robotic exoskeleton systems developed in the authors' lab (University of Washington, University of California Santa Cruz, University of California Los Angeles). Related research has also been covered.

REFERENCES

[1] P. Langhorne, J. Bernhardt, G. Kwakkel, Stroke rehabilitation, Lancet 377 (2011) 1693–1702.
[2] E.J. Benjamin, et al., Heart disease and stroke statistics-2017 update: a report from the American Heart Association, Circulation 135 (10) (2017) e146–e603.
[3] B.H. Dobkin, Rehabilitation after stroke, N. Engl. J. Med. 352 (16) (2005) 1677–1684.
[4] J. Rosen, Natural Integration of a Human Arm/Exoskeleton System, Tel-Aviv University, 1997.
[5] J. Rosen, M.B. Fuchs, M. Arcan, Performances of hill-type and neural network muscle models-toward a myosignal-based exoskeleton, Comput. Biomed. Res. 32 (5) (1999) 415–439.
[6] J. Rosen, M. Brand, M.B. Fuchs, M. Arcan, A myosignal-based powered exoskeleton system, IEEE Trans. Syst. Man, Cybern. Part A Syst. Humans 31 (3) (2001) 210–222.
[7] J.C. Perry, J. Rosen, Case study: an upper limb powered exoskeleton, in: J.L. Pons (Ed.), Wearable Robots: Biomechatronic Exoskeletons, John Wiley & Sons, 2008.
[8] J.C. Perry, J. Rosen, S. Burns, Upper-limb powered exoskeleton design, IEEE/ASME Trans. Mechatronics 12 (4) (2007) 408–417.
[9] J.C. Perry, J.M. Powell, J. Rosen, Isotropy of an upper limb exoskeleton and the kinematics and dynamics of the human arm, Appl. Bionics Biomech. 6 (2) (2009) 175–191.

[10] J. Rosen, J.C. Perry, N. Manning, S. Burns, B. Hannaford, The human arm kinematics and dynamics during daily activities - toward a 7 DOF upper limb powered exoskeleton, in: 2005 International Conference on Advanced Robotics, ICAR '05, Proceedings, 2005, no. July, pp. 532–539.
[11] J.C. Perry, J. Rosen, Design of a 7 degree-of-freedom upper-limb powered exoskeleton, in: Biomedical Robotics and Biomechatronics, 2006. BioRob 2006. The First IEEE/RAS-EMBS International Conference on, 2006, pp. 805–810.
[12] J.C. Perry, Design and development of a 7 degree-of-freedom powered exoskeleton for the upper limb, University of Washington, 2006.
[13] J. Rosen, J.C. Perry, Upper limb powered exoskeleton, Int. J. Humanoid Robot. 04 (03) (2007) 529–548.
[14] E. Cavallaro, J. Rosen, J.C. Perry, S. Burns, B. Hannaford, Hill-based model as a myoprocessor for a neural controlled powered exoskeleton arm - parameters optimization, in: Proceedings of the 2005 IEEE International Conference on Robotics and Automation, 2005, no. April, pp. 4525–4530.
[15] E.E. Cavallaro, J. Rosen, J.C. Perry, S. Burns, Real-time myoprocessors for a neural controlled powered exoskeleton arm, IEEE Trans. Biomed. Eng. 53 (11) (2006) 2387–2396.
[16] L.M. Miller, Gravity Compensation for a 7 Degree of Freedom Powered Upper Limb Exoskeleton, University of Washington, 2006.
[17] W. Yu, J. Rosen, A novel linear PID controller for an upper limb exoskeleton, in: Proceedings of the IEEE Conference on Decision and Control, 2010, pp. 3548–3553.
[18] W. Yu, J. Rosen, X. Li, PID admittance control for an upper limb exoskeleton, in: 2011 American Control Conference, 2011, pp. 1124–1129.
[19] W. Yu, J. Rosen, Neural PID control of robot manipulators with application to an upper limb exoskeleton, IEEE Trans. Cybern. 43 (2) (2013) 673–684.
[20] L.M. Miller, Comprehensive Control Strategies for a Seven Degree of Freedom Upper Limb Exoskeleton Targeting Stroke Rehabilitation, University of Washington, 2012.
[21] H. Kim, Systematic Control and Application for 7 DOF Upper-Limb Exoskeleton, University of California, Santa Cruz, 2012.
[22] Y. Shen, Control and Dynamic Manipulability of a Dual-Arm/Hand Robotic Exoskeleton System (EXO-UL8) for Rehabilitation Training in Virtual Reality, University of California, Los Angeles, 2019.
[23] Y. Shen, P.W. Ferguson, J. Ma, J. Rosen, Upper limb wearable exoskeleton systems for rehabilitation: state of the art review and a case study of the EXO-UL8 - dual-arm exoskeleton system, in: Wearable Technology in Medicine and Health Care, Elsevier, 2018, pp. 71–90. http://dx.doi.org/10.1016/B978-0-12-811810-8.00004-X.
[24] Y. Shen, J. Ma, B. Dobkin, J. Rosen, Asymmetric dual arm approach for post stroke recovery of motor functions utilizing the EXO-UL8 exoskeleton system: a pilot study, 2018 40th Annual International Conference of the IEEE Engineering in Medicine and Biology Society (EMBC), 2018, pp. 1701–1707. http://dx.doi.org/10.1109/EMBC.2018.8512665.
[25] Y. Shen, J. Sun, J. Ma, J. Rosen, Admittance control scheme comparison of EXO-UL8: a dual-arm exoskeleton robotic system, 2019 IEEE 16th International Conference on Rehabilitation Robotics (ICORR), 2019, pp. 611–617. http://dx.doi.org/10.1109/ICORR.2019.8779545.
[26] P.W. Ferguson, B. Dimapasoc, Y. Shen, J. Rosen, Design of a hand exoskeleton for use with upper limb exoskeletons, in: M.C. Carrozza, S. Micera, J.L. Pons (Eds.), Wearable Robotics: Challenges and Trends, Springer International Publishing, Cham, 2019, pp. 276–280.
[27] L.M. Miller, J. Rosen, Comparison of multi-sensor admittance control in joint space and task space for a seven degree of freedom upper limb exoskeleton, in: Proceedings of the 2010 3rd IEEE RAS & EMBS International Conference on Biomedical Robotics and Biomechatronics, 2010, pp. 70–75.
[28] H. Kim, L.M. Miller, A. Al-Refai, M. Brand, J. Rosen, Redundancy resolution of a human arm for controlling a seven DOF wearable robotic system, in: Proceedings of the Annual International Conference of the IEEE Engineering in Medicine and Biology Society, EMBS, 2011, pp. 3471–3474.

[29] L.M. Miller, H. Kim, J. Rosen, Redundancy and joint limits of a seven degree of freedom upper limb exoskeleton, in: Proceedings of the Annual International Conference of the IEEE Engineering in Medicine and Biology Society, EMBS, 2011, pp. 8154–8157.
[30] H. Kim, L.M. Miller, N. Byl, G.M. Abrams, J. Rosen, Redundancy resolution of the human arm and an upper limb exoskeleton, IEEE Trans. Biomed. Eng. 59 (6) (2012) 1770–1779.
[31] H. Kim, J.R. Roldan, Z. Li, J. Rosen, Viscoelastic model for redundancy resolution of the human arm via the swivel angle: applications for upper limb exoskeleton control, in: Conference Proceedings: ... Annual International Conference of the IEEE Engineering in Medicine and Biology Society. IEEE Engineering in Medicine and Biology Society. Annual Conference, 2012, pp. 6471–6474.
[32] H. Kim, L.M. Miller, Z. Li, J.R. Roldan, J. Rosen, Admittance control of an upper limb exoskeleton - reduction of energy exchange, in: Proceedings of the Annual International Conference of the IEEE Engineering in Medicine and Biology Society, EMBS, 2012, pp. 6467–6470.
[33] H. Kim, Z. Li, D. Milutinović, J. Rosen, Resolving the redundancy of a seven DOF wearable robotic system based on kinematic and dynamic constraint, in: Proceedings of International Conference on Robotics and Automation, 2012, pp. 305–310.
[34] B. Kashi, M. Brand, J. Rosen, I. Avrahami, Synthesizing two criteria for redundancy resolution of human arm in point tasks, in: 2011 Third World Congress on Nature and Biologically Inspired Computing (NaBIC), 2011, 63–68.
[35] Z. Li, J.R. Roldan, D. Milutinovic, J. Rosen, The rotational axis approach for resolving the kinematic redundancy of the human arm in reaching movements, in: Proceedings of the Annual International Conference of the IEEE Engineering in Medicine and Biology Society, EMBS, 2013, no. 2, pp. 2507–2510.
[36] Z. Li, H. Kim, D. Milutinović, J. Rosen, Synthesizing redundancy resolution criteria of the human arm posture in reaching movements, in: Redundancy in Robot Manipulators and Multi-Robot Systems, 2013, 201–240.
[37] Z. Li, D. Milutinovic, J. Rosen, Spatial map of synthesized criteria for the redundancy resolution of human arm movements, IEEE Trans. Neural Syst. Rehabil. Eng. 23 (6) (2015) 1020–1030.
[38] Z. Li, J.R. Roldan, D. Milutinovi, Task-relevance of grasping-related degrees of freedom in reach-to-grasp movements, in: 36th Annual International Conference of the IEEE Engineering in Medicince and Biology Society, EMBS, 2014, pp. 6903–6906.
[39] Z. Li, K. Gray, J.R. Roldan, D. Milutinović, J. Rosen, The joint coordination in reach-to-grasp movements, in: IEEE International Conference on Intelligent Robots and Systems, 2014, pp. 906–911.
[40] Y. Shen, B.P. Hsiao, J. Ma, J. Rosen, Upper limb redundancy resolution under gravitational loading conditions: arm postural stability index based on dynamic manipulability analysis, 2017 IEEE-RAS 17th International Conference on Humanoid Robotics (Humanoids), 2017, pp. 332–338. http://dx.doi.org/10.1109/HUMANOIDS.2017.8246894.
[41] B. Kashi, I. Avrahami, J. Rosen, M. Brand, A bi-criterion model for human arm posture prediction, in: 2012 World Congress on Medical Physics and Biomedical Engineering, 2012, 1–4.
[42] H. Kim, J. Rosen, Predicting redundancy of a 7 DOF upper limb exoskeleton toward improved transparency between human and robot, J. Intell. Robot. Syst. 80 (2015).
[43] D. Milutinović, J. Rosen (Eds.), Redundancy in Robot Manipulators and Multi-Robot Systems, Springer, 2013.
[44] Z. Li, The Synergy of Human Arm and Robotic System, University of California, Santa Cruz, 2014.
[45] K.J. Sullivan, et al., Fugl-Meyer assessment of sensorimotor function after stroke: standardized training procedure for clinical practice and clinical trials, Stroke 42 (2) (2011) 427–432.
[46] A. Feldman, Y. Shen, J. Rosen, Modeling of joint synergy and spasticity in stroke patients to solve arm reach tasks, 2017 IEEE Signal Processing in Medicine and Biology Symposium (SPMB), 2017 IEEE, 2017, pp. 1–3. http://dx.doi.org/10.1109/SPMB.2017.8257046.

[47] M. Simkins, A.H. Al-Refai, J. Rosen, Upper limb joint space modeling of stroke induced synergies using isolated and voluntary arm perturbations, IEEE Trans. Neural Syst. Rehabil. Eng. 22 (3) (2014) 491–500.
[48] M. Simkins, A. Burleigh Jacobs, J. Rosen, Rhythmic affects on stroke-induced joint synergies across a range of speeds, Exp. Brain Res. 229 (4) (2013) 517–524.
[49] M. Simkins, A.B. Jacobs, N. Byl, J. Rosen, Stroke-induced synergistic phase shifting and its possible implications for recovery mechanisms, Exp. Brain Res. 232 (11) (2014) 3489–3499.
[50] A.H. Al-Refai, Objectively Characterized Linear Model of Stroke Induced Joint Synergies in Relation to Clinical Measures, University of California, Santa Cruz, 2012.
[51] M. Simkins, Human Movement Synergies of the Upper Extremities, University of California, Santa Cruz, 2013.
[52] J.H. Cauraugh, J.J. Summers, Neural plasticity and bilateral movements: a rehabilitation approach for chronic stroke, Prog. Neurobiol. 75 (5) (2005) 309–320.
[53] M. Simkins, H. Kim, G. Abrams, N. Byl, J. Rosen, Robotic unilateral and bilateral upper-limb movement training for stroke survivors afflicted by chronic hemiparesis, in: IEEE International Conference on Rehabilitation Robotics, 2013, pp. 1–6.
[54] M. Simkins, N. Byl, H. Kim, G. Abrams, J. Rosen, Upper limb bilateral symmetric training with robotic assistance and clinical outcomes for stroke: a pilot study, Int. J. Intell. Comput. Cybern. 9 (1) (2016) 83–104.
[55] N.N. Byl, et al., Chronic stroke survivors achieve comparable outcomes following virtual task specific repetitive training guided by a wearable robotic orthosis (UL-EXO7) and actual task specific repetitive training guided by a physical therapist, J. Hand Ther. 26 (4) (2013) 343–352.
[56] J. Rosen, D. Milutinović, L.M. Miller, M. Simkins, H. Kim, Z. Li, Unilateral and bilateral rehabilitation of the upper limb following stroke via an exoskeleton, in: P. Artemiadis (Ed.), Neuro-Robotics: From Brain Machine Interfaces to Rehabilitation Robotics, Dordrecht, Springer Netherlands, 2014, pp. 405–446.
[57] H. Kim, et al., Kinematic data analysis for post-stroke patients following bilateral versus unilateral rehabilitation with an upper limbwearable robotic system, IEEE Trans. NEURAL Syst. Rehabil. Eng. 21 (2) (2013) 153–164.
[58] J.R.U. Roldan, D. Milutinovic, Z. Li, J. Rosen, A low-dimensional dissimilarity analysis of unilateral and bilateral stroke-impacted hand trajectories, J. Dyn. Syst. Meas. Control 138 (11) (2016) 111007.
[59] Z. Li, K. Hauser, J.R. Roldan, D. Milutinovic, J. Rosen, A novel method for quantifying arm motion similarity, in: Proceedings of the Annual International Conference of the IEEE Engineering in Medicine and Biology Society, EMBS, 2015, pp. 5716–5719.
[60] M. Simkins, I. Fedulow, H. Kim, G. Abrams, N. Byl, J. Rosen, Robotic rehabilitation game design for chronic stroke, Games Health J. 1 (6) (2012) 422–430.
[61] M. Simkins, J.R. Roldan, H. Kim, G. Abrams, N. Byl, J. Rosen, Kinematic analysis of virtual reality task intensity induced by a rehabilitation robotic system in stroke patients, in: Proceedings of ASME 2013 Dynamic Systems and Control Conference 2013, 2013, pp. 1–7.

This page intentionally left blank

CHAPTER

6 PRISM: DEVELOPMENT OF A 2-DOF DUAL-FOUR-BAR EXOSKELETON SHOULDER MECHANISM TO SUPPORT ELEVATION, DEPRESSION, PROTRACTION, AND RETRACTION

Joel C. Perry, Chris K. Bitikofer, Parker W. Hill, Shawn T. Trimble and Eric T. Wolbrecht
Mechanical Engineering Department, University of Idaho, Moscow, ID, United States

6.1 INTRODUCTION

As one of the leading causes of long-term functional deficits in the arm and hand, the annual incidence of stroke is about 800,000 in the United States and about 42 million globally [1]. Losses in arm function and mobility occur in some 85% of strokes and persist at least 3–6 months after stroke in 55%–75% of cases [2]. This number is projected to rise over the next several decades due to the effect of increases in the following four factors: (1) life expectancies, (2) prevalence of stroke with age, (3) number of baby-boomers reaching the age of higher prevalence, and (4) post-stroke survival rates. These growing trends place a large burden on our healthcare system and increase the need for more therapists to perform hands-on and physically demanding rehabilitation treatments. The introduction of robotics onto the therapeutic stage [3–6] brings welcomed characteristics including high strength, precision, and repeatability. Research has demonstrated the efficacy of robotic therapy to match or exceed conventional therapy when provided in equivalent doses [7], and that robotic devices can facilitate far greater numbers of therapeutic repetitions in a single therapy session than can be achieved by therapists alone [8]. Robotics also offer improved elements of quantitative measurement which give meaningful feedback to patients and care providers. This feedback has major implications for care, offering the ability to guide and individualize therapy, gauge compliance, motivate progress, and justify continuation of care to insurers. Furthermore, robotic measures give researchers new ways to study therapy hypotheses and evolve robotic device design. Ensuring accuracy of measurement is therefore of the utmost importance, and is significantly linked to the appropriateness of the robot's design in terms of fit and function to the needs of the human users.

Wearable Robotics. DOI: https://doi.org/10.1016/B978-0-12-814659-0.00006-0

6.1.1 REHABILITATION ROBOTICS: EXOSKELETON VERSUS END-EFFECTOR

Assessing and rehabilitating the deficits caused by stroke and other cerebrovascular accidents has been a major motivating factor behind the proliferation of rehabilitation robotics over the past two decades. In the design and development of robotics for the upper extremity, both exoskeleton [9–13] and end-effector [14–17] approaches are common. Exoskeletons provide structural links in close proximity to, and along the length of, the arm. Their kinematics mimic anatomical movements by aligning robot joint axes with approximations of human joint axes and maintaining alignment throughout the user's motion. End-effector robots, on the other hand, attach to the user at the hand and/or forearm, and may use any number of joint configurations to enable an end-effector workspace that coincides with a subset of the user's hand and/or forearm workspace.

In both end-effector and exoskeleton design approaches, safe and comfortable operation requires that robot-induced movements remain within normal ranges of motion at all times and across all joints of the driven human limb. Different approaches can be taken to ensure anatomically appropriate joint motions, which can involve direct control of the joints or, in other cases, an intentional lack of control over specific joints. The latter approach of adding passive joints into the design is referred to as underactuation and is most often applied in robotic hands [18,19] and legs [20]. End-effector–based systems commonly control an end-point position while the inclusion of passive degrees-of-freedom (DOFs) leave some aspect of arm orientation underconstrained. Exoskeleton-based systems, however, rely on proper alignment between joints of the exoskeleton and user [11]. The user must be fully constrained to the device such that the locations and orientations of the user's anatomical joints are reasonably known.

Consequently, maintaining proper alignment between the joints of the robotic device and the joints of the human user is one of the principal challenges in exoskeleton design. Problems resulting from inadequate joint alignment can include excessive or unwanted forces exerted on the patient and/or exoskeleton, inaccurate measurements, and increased risk of joint injuries such as shoulder subluxation (i.e., partial dislocation). In an attempt to address this concern, current exoskeleton designs are beginning to incorporate features that better accommodate slight misalignments, or that attempt to eliminate them entirely. This has been attempted in the wrist [21], the elbow [22,23], and the shoulder [9,24–26].

While allowing proper alignment, or accommodating for misalignment, is important for all users of exoskeletons, it is especially important when used with individuals having acute-stage neurological impairments (e.g., 1–2 weeks poststroke). A common early sequela poststroke is muscular flaccidity (i.e., no tone) followed by hypotonia (i.e., low tone) [27], both of which lead to instability in the joints and increased risk of injury if not properly supported [9]. This is of particular importance in the shoulder complex where the highest risk for subluxation occurs [28].

6.1.2 EXOSKELETON SHOULDER BACKGROUND

6.1.2.1 State of the art

Over the past decade, a handful of systems have provided varying solutions to address some of the additional DOFs provided by the shoulder complex, but few account for full shoulder mobility [29–33]. In the healthy shoulder, articulation is a combination of four joints: the glenohumeral (GH), acromioclavicular (AC), and sternoclavicular (SC) synovial joints, and a scapulothoracic

(ST) "false" joint formed by musculature between the scapula and thoracic cage (see Fig. 6.1). Together the four joints of the shoulder girdle provide the humerus with the freedom to move within a nearly hemispherical workspace with a rather nonlinear center of rotation [35]. Although the overall shoulder structure has been previously represented by numerous models [36], its replication with an anthropomorphic exoskeleton remains a significant design challenge.

In total, the shoulder complex consists of 5 DOFs [36], but many designs account for only three. In an attempt to simplify the shoulder, the most popular approach with robotic systems has been to represent the shoulder as a 3-DOF spherical joint, mimicking the behavior of the GH joint, and neglecting the articulations of the ST, SC, and AC joints. However, these articulations are vital to achieving full range of motion (ROM) in the shoulder; without them, exoskeletal shoulder alignment is reasonably maintained over a limited range of humeral elevation ($<$90 degrees), and leads to increased misalignment with higher levels of humeral elevation above horizontal.

Recognizing that increased humeral elevation has a nonlinear relationship to SC, AC, and ST articulation, referred to as scapulohumeral rhythm, shoulder designs have been developed with variations to the standard 3-DOF spherical arrangement in order to further reduce misalignments and increase the allowable workspace. A few of the more notable systems include the MGA, ARMin, MEDARM, and HARMONY exoskeletons (Fig. 6.2), described below.

The *MGA exoskeleton*, built in 2005, is a 6-DOF upper-limb exoskeleton with a 4-DOF shoulder. The MGA models the GH joint as a ball and socket, with three actuated DOFs. A fourth DOF is placed behind the patient in line with the SC joint (Fig. 6.2), which allows for elevation/depression of the shoulder girdle [37,41]. The addition of a 1-DOF SC joint allows for increased GH mobility that supports shoulder elevation (upward) and depression (downward).

The *ARMin I*, *II*, and *III*, prototypes developed between 2005 and 2008, each used 3-DOF shoulders with variations of additional shoulder DOFs. The ARMin I used a passive gravity-balanced linear DOF to support vertical translation of the entire exoskeleton, similar to elevation/depression; however, being a passive DOF, the system's position was not actively determined and became problematic for patients with risk of shoulder subluxation [9]. The ARMin II coupled the passive shoulder elevation/depression DOF with humeral elevation. This achieves a substantially similar result to the single SC-aligned DOF used in the MGA exoskeleton. The ARMin III took this coupling approach a step further by replacing the vertical translation of the GH joint by a circular path that was numerically optimized to minimize anatomical error with typical humeral head movement. Protraction/retraction support was not added as the authors noted that misalignment in this direction could be overcome by torso movements from the patient. It is worth noting that the ARMin III is the only exoskeleton of those discussed here that is commercially available (as the ArmeoPower); so far, the other systems exist in research settings only.

The *MEDARM* is a 6-DOF exoskeleton with a 5-DOF shoulder that claims to be the first rehabilitation robot to fully account for shoulder movement [36]. Two independent DOFs are aligned with the SC joint, one positioned behind the user for elevation/depression and the other positioned above the user for protraction/retraction. As a result, the entirety of shoulder girdle motion is accommodated.

The *HARMONY* is a dual upper-limb exoskeleton developed for rehabilitation. Like the MEDARM, the HARMONY proposes a novel solution to the shoulder mobility problem [34,42]. Scapulohumeral rhythm is accounted for by way of a parallelogram mechanism positioned behind the patient. The parallelogram serves to provide protraction/retraction of the joint while a single

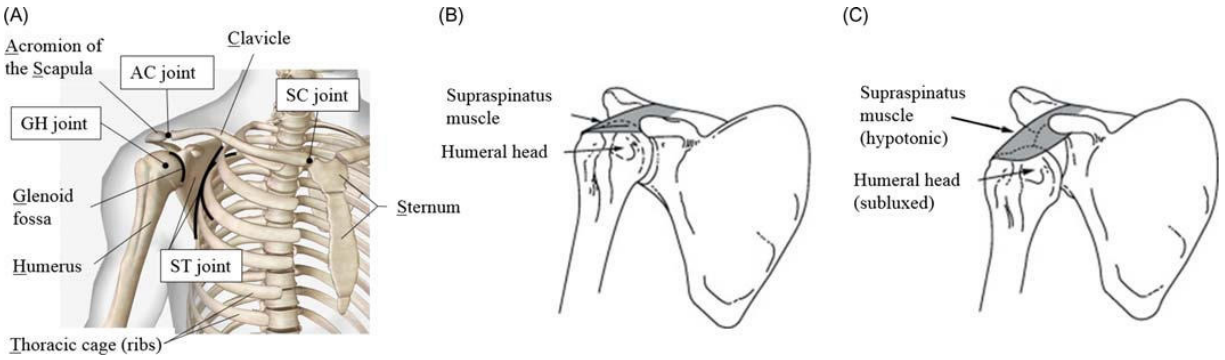

FIGURE 6.1

The shoulder complex (A) is comprised of three bones: the clavicle, humerus, and scapula. Four joints form the entire shoulder girdle: sternoclavicular, acromioclavicular, glenohumeral, and the scapulothoracic joints. In the healthy shoulder, the supraspinatus muscle is a major contributor to proper shoulder stability (B). Under hypotonic conditions, flaccidity of the musculature results in humeral head subluxation (C).

(A) Adapted from D.A. Neumann, Kinesiology of the Musculoskeletal System-E-Book: Foundations for Rehabilitation, Elsevier Health Sciences, 2013 [34]. (B and C) Adapted from M. Murie-Fernandez, M.C. Iragui, V. Gnanakumar, M. Meyer, N. Foley, R. Teasell, Painful hemiplegic shoulder in stroke patients: causes and management, Neurología (English Ed.) 27 (4) (2012) 234–244.

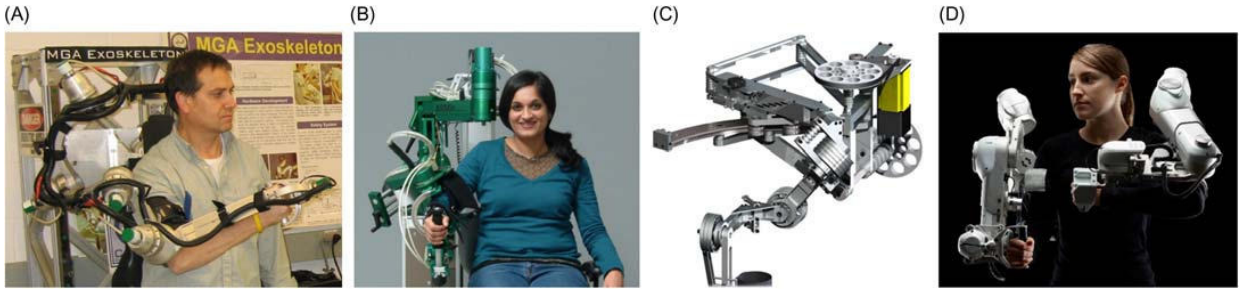

FIGURE 6.2

Notable exoskeleton arms that incorporate aspects of SC, AC, and/or ST articulation: (A) the MGA exoskeleton [37], (B) the ARMin III [38], (C) the MEDARM [39], and (D) the HARMONY [40].

revolute joint permits elevation/depression. Motion of the GH joint is accomplished through three DOFs, but one will note that the angles between the axes are not orthogonal as in most other exoskeleton designs.

Each of the above exoskeletons provide 3 DOFs to support GH ROM, but variations between axes orientation can clearly be seen. In the ARMin, shoulder internal/external rotation is the third GH axis (GH3), while in the others, internal/external rotation is achieved through a combination of all three GH axes (GH1, GH2, and GH3). It is also worth noting that the selection and placement of the first axis has major implications not only on the allowable ROM of the resulting exoskeleton shoulder, but also on the location (or existence) of workspace singularities. A singularity can occur when two axes are aligned, effectively eliminating one of the DOFs of the device. The effect of a singularity is apparent both near and at the alignment of two joint axes as the manipulability of the device degrades. In mechanical systems, a singularity can manifest either as "gimbal lock", in which case axial alignment prevents the mechanism from being able to move in a given direction, or as an underconstrained system, in which case axial alignment allows multiple movements to achieve the same result. Both are problematic for proper control of the end-effector. Placing the first GH joint (GH1) directly above the shoulder, as was done in the ARMin III, has the potential to create three singularities when the arm is straight down along the side of the body; one between GH1 and GH3 (internal external rotation), a second between GH3 and forearm pronosupination (PS), and a third between GH1 and PS. In the axial configurations used in the MEDARM and MGA exoskeleton designs, the point of singularity between GH1 and GH3 have been placed in hard-to-reach locations on the edge of, or entirely outside the workspace of the human arm. This minimizes the risk that the singularity is reached and therefore reduces the negative effects of the singularity on the mechanism, such as poor manipulability. In the HARMONY design, it may be noted that the angle between GH1 and GH2, and between GH2 and GH3 are not 90 degrees as in most other exoskeletons. While this does prevent direct alignment between axes GH1 and GH3, it does not prevent the singularity from occurring. Some discussion on the placement of the axes GH1, GH2, and GH3 can be found in Ref. [42].

Although the advantages and disadvantages behind placing the GH axes at various locations is not the focus of this paper, it is important to note that their selection does impact the device's ROM, manipulability, and relative ease (or ability) to incorporate additional proximal DOFs, such as the SC joint, in order to allow a more anthropomorphic shoulder actuation. As can be seen in the designs of Fig. 6.2, the incorporation of SC joint axes into an exoskeleton arm can take up substantial real estate behind or above the user, even to the point where it compromises GH joint ROM. The HARMONY implementation is a great example of an elegant low-profile design that incorporates all 5 shoulder DOFs; however, the elegance comes at the cost of limited bilateral shoulder ROM due to the close placement of motors, and as a result, shoulder abduction is unable to reach the ROM in which the additional SC DOFs contribute most (>90 degrees). MEDARM's design clearly precludes the ability to extend this device to a bilateral version due to the placement of hardware that drives the exoskeleton's SC axes (SC1 and SC2) whose joints must align with the anatomical SC joint.

6.1.2.2 3-DOF versus 5-DOF shoulder

As previously mentioned, being able to measure the arm orientation accurately is highly important for assessment purposes. Knowing that misalignments alter the accuracy of measurements, adding a

4th or 5th joint to the shoulder is advantageous. Why not just add a coupled DOF to elevate the shoulder along with humeral elevation instead of adding another motor? While this approach does closely match healthy kinematics of the shoulder girdle, impaired individuals do not exhibit healthy kinematics. The shoulder is one of the joints where much of the impairment is evident. Muscular weakness, cocontraction, spasticity, and abnormal joint torque couplings at the shoulder make it difficult for many patients to control abduction without elevating the humeral head via SC, AC, and ST articulation. In this case, the elevation of the humeral head is not coupled with elevation of the humerus and would result in undesirable and potentially harmful forces and torques on the individual if exhibited in an exoskeleton with a fixed or floating 3-DOF GH joint. For assessment purposes, the inclusion of a 2-DOF anthropomorphic clavicle to a 3-DOF GH joint has strong merit.

6.1.2.3 Bilateral versus unilateral shoulder designs

In recent years, there has been a growing interest in bilateral task training [43–47], showing benefits over unilateral and other types of training. Similarly, bilateral assessment offers many advantages over unilateral assessment. It is nothing new to the clinical community who routinely compare impaired and intact sides of the body, but is often neglected in robotic systems for economic reasons. The ARMin provides a design which can be reconfigured for either arm, whereas the HARMONY provides mirrored parts that achieve a left and right version. The HARMONY is one of the few exoskeletons since the EXO-UL7 [11] that was developed from the start for bilateral use with impaired users. The majority of other systems would require substantial redesign to incorporate SC and AC shoulder joints that allow a design with simultaneous bilateral capability.

6.1.3 OVERVIEW

In this work, we propose a novel mechanism that mimics the biomechanics of the clavicle about the AC and SC joints in order to add protraction/retraction and elevation/depression movements to spherical shoulder designs in existing robotic exoskeletons. The resulting mechanism uses a unique dual four-bar spatial design to provide 2 DOFs of shoulder mobility. The design has been termed "PRISM" (Parallel Remote Inclusion of Shoulder Mobility) and will be part of a new exoskeleton arm instrument called BLUE SABINO that takes advantage of key aspects from previous exoskeleton designs including EXO-UL7 [11], EXO-UL8 [48], LIMPACT [23], and HARMONY [42]. The BLUE SABINO concept, the mobility requirements for unimpaired shoulders, and the kinematics of the PRISM mechanism are presented below in Section 6.2, followed by the final design and discussion in Sections 6.3 and 6.4.

6.2 METHODS: PRISM DEVELOPMENT

In the following methods, the approach has been aimed at addressing the needs of a 5-year NSF project called BLUE SABINO. The overarching goal of the project is to develop a new instrument for comprehensive assessment of neurological impairment affecting functional mobility in the arm or hand. The project involves development of two full-arm exoskeletons (shoulder, elbow, wrist, and hand) with a fully integrated EMG/EEG acquisition system. The exoskeleton is modeled after

a previous exoskeleton design, the EXO-UL8, which utilizes a 3-DOF shoulder joint, adjustable link lengths, and direct Harmonic Drive actuation. To improve upon the anthropomorphic fit between user and device throughout the workspace, the PRISM mechanism is developed in the sections that follow.

6.2.1 BLUE SABINO CONCEPT

BLUE SABINO is a rather lengthy but technically appropriate acronym for BiLateral Upper-limb Exoskeleton for Simultaneous Assessment of Biomechanical and Neuromuscular Output. The project aims to create an instrument to help researchers and scientists improve upon our understanding of the fundamental contributors to neurological impairment. A schematic of the overall instrument and interior architecture is shown in Fig. 6.3. As depicted in the figure, the instrument architecture is composed of a task environment, a biosignal acquisition system, a data processing unit, and a storage database. The biosignal acquisition system interfaces with the human at three noninvasive levels: cerebral cortex (visual and motor), neuromuscular (arm musculature), and musculoskeletal (arm and hand exterior). The musculoskeletal interface represents the physical human−machine interface to the exoskeleton.

The BLUE SABINO exoskeleton will have a set of bilateral (left and right) exoskeleton arms supporting anatomical articulations of the shoulder, elbow, wrist, thumb, index finger, and

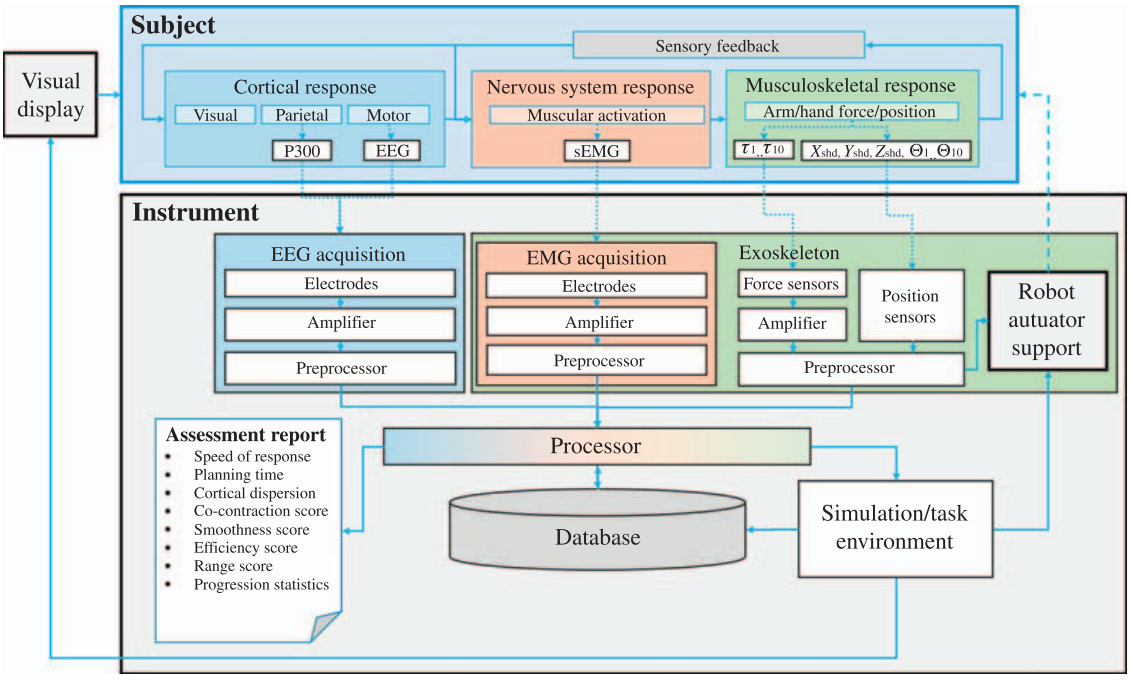

FIGURE 6.3

Instrument architecture with relation to the human subject and the acquisition of brain signals (*blue*), muscle signals (*red*), and arm movements and forces (*green*).

middle/ring/pinky finger combination. In total, each arm includes 15 active (i.e., motorized) and 8 passive (i.e., nonmotorized) joints, or DOFs. For development, exoskeleton subassemblies are divided into a 2-DOF passive base, a 2-DOF active shoulder, a 7-DOF active arm, and a 12-DOF hand (six active, six passive). The arm exoskeleton connects to the user at key points along the arm and hand and must be designed around desired electrode placement in order to minimize the introduction of movement artifacts in the SEMG signals. The bilateral aspect is intended to provide intrasubject measures between impaired and unimpaired limb (in the case of hemiparetic stroke) as well as assessment in performing bilateral tasks. Previous 7-DOF and 8-DOF exoskeleton arms [11,43,49], developed in part by the authors, provide a starting point to the arm and hand design in order to allow a greater focus on extending functionality to SC/AC and finger/thumb articulations.

6.2.2 EXO-UL8 DESIGN APPROACH

The *EXO-UL8* is the second generation of an earlier EXO-UL7 arm, but with an added DOF at the hand for grasp-release training. The EXO-UL7, (aka, CADEN-7) was one of the earliest examples of a 7-DOF exoskeleton with a lightweight and low-profile design (Fig. 6.4A). Features include a cable-driven power transmission from stationary base-mounted actuators, shoulder singularity avoidance through peripheral placement, and open bearing designs at both the upper arm and the forearm. Drawbacks to the system include (1) complexity of cable routing repair in the event of cable rupture, (2) lack of adjustability in arm lengths, (3) a stationary GH joint, (4) no hand grasp functionality, and (5) high-cost precision enclosures around the arm to allow axial rotation. As a second-generation system, the EXO-UL8 (Fig. 6.4B) addressed several of the potential disadvantages of the EXO-UL7 by (1) replacing cable transmissions with direct-drive integrated harmonic drive actuation, (2) adding length adjustment mechanisms for the upper and lower arm, and (3) adding a 1-DOF hand grasp module. It also addressed important strength and robustness concerns

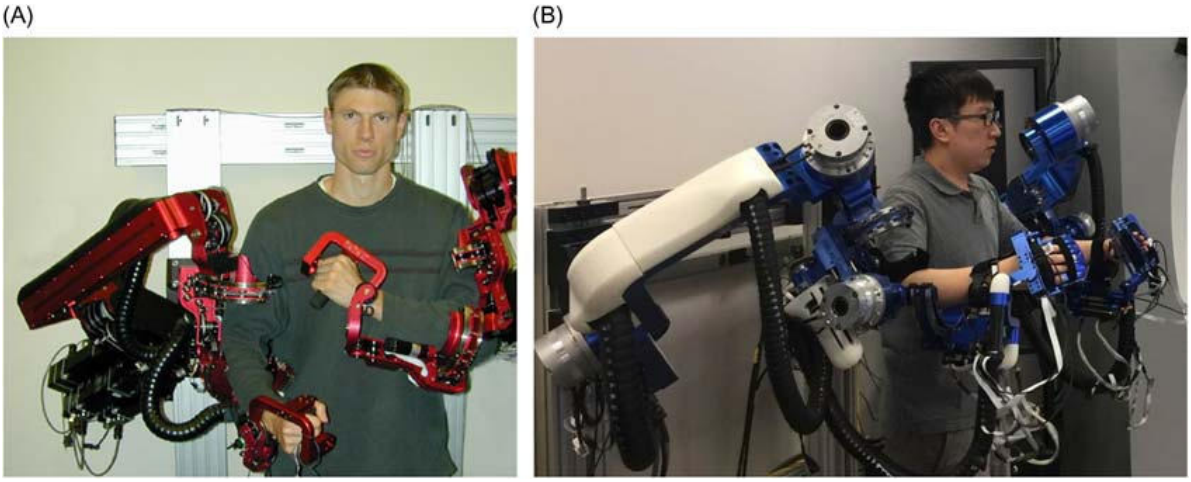

FIGURE 6.4

The EXO-UL7 (A) and EXO-UL8 (B) exoskeletons serve as previous iterations to the BLUE SABINO exoskeleton design.

following user testing with both healthy and impaired populations. The shoulder in both designs was represented by a spherical joint composed of three orthogonal axes intersecting at the estimated center of the shoulder GH joint. The first shoulder axis, GH1, intersects the inferior posterolateral aspect of the shoulder, achieving a combination of abduction and flexion. The second shoulder axis, GH2, is orthogonal to GH1 and sits on the anterolateral aspect of the shoulder when the arm is straight down. GH3 is aligned with the long axis of the humerus. As a result of having already been vetted with stroke patients, the EXO-UL7, with modifications from the EXO-UL8 redesign, was taken as the starting configuration for the BLUE SABINO design.

6.2.3 SHOULDER RANGE OF MOTION REQUIREMENTS ESTIMATION

The requirements at the shoulder depend to some degree on the population of interest and their impairment characteristics. The target population in this case suffers from neurological impairment as a result of conditions such as stroke or cerebral palsy; furthermore, it is necessary to be able to assess both impaired and unimpaired limbs for baseline comparisons. For these reasons, the desired ROM of the system is the full ROM of the unimpaired shoulder including GH, SC, and AC joint contributions. While not all aspects of full ROM will be necessary for impaired limbs, the SC and AC joint inclusion will allow accurate measurement in a greater array of exhibited neuropathies and compensatory strategies, as well as accurate assessment of subjects' unimpaired ipsilesional sides, in the case of stroke.

To assess just how much mobility is needed to accommodate a healthy shoulder girdle, an activities-of-daily-living (ADLs) database [49] was used to estimate the translation of the GH joint during a variety of daily tasks. Most tasks were performed while seated at a desk with target locations for pick and place reaching tasks labeled on the desk and shelf as shown in Fig. 6.5. The dataset was collected using a 12-camera VICON motion capture system that tracked the Cartesian locations of seven markers on a subject at a rate of 120 Hz. The system maps the locations of the markers to an internal kinematic model and exports both Euler angle rotations for rigid bodies representing the arm, and Cartesian locations of the centers of rotation of the shoulder, elbow, and wrist.

The kinematic motions for 24 ADLs were captured for six subjects whose ages ranged from 20 to 41 years. Three of the subjects were male and three were female. Mean and standard deviations of height, weight, and age were 1.72 ± 0.08 m, 76.2 ± 23.1 kg, and 26.2 ± 7.7 years, respectively. Tasks were broken into subgroups of Reaching, Functional ADLs, Eating and Drinking, and Hygiene as follows:

1. Reaching (actions 1−7): Placing hand on desk (RP to Dh), moving an object between desktop positions (D1R to D1L, D0 to D2), *moving an object between shelf positions (S2L to S2R)*, *combination shelf/desktop object motions (D1R to S2L, D1L to S2R, D1 to S2)*.
2. Functional ADLs (actions 8−15): *Opening and closing a door*/cabinet/drawer, answering a table-mounted phone (Dp), overhand/underhand stirring with a utensil (D1), pouring from a pitcher to a cup (Dp to Dc), and pouring from a cup to a pitcher (D1R to D1).
3. Eating and drinking (actions 16−19): Normal eating with a fork (D0), *powered grasp eating with a fork (D0)*, eating with right hand (D0), and drinking from a cup (Dc).

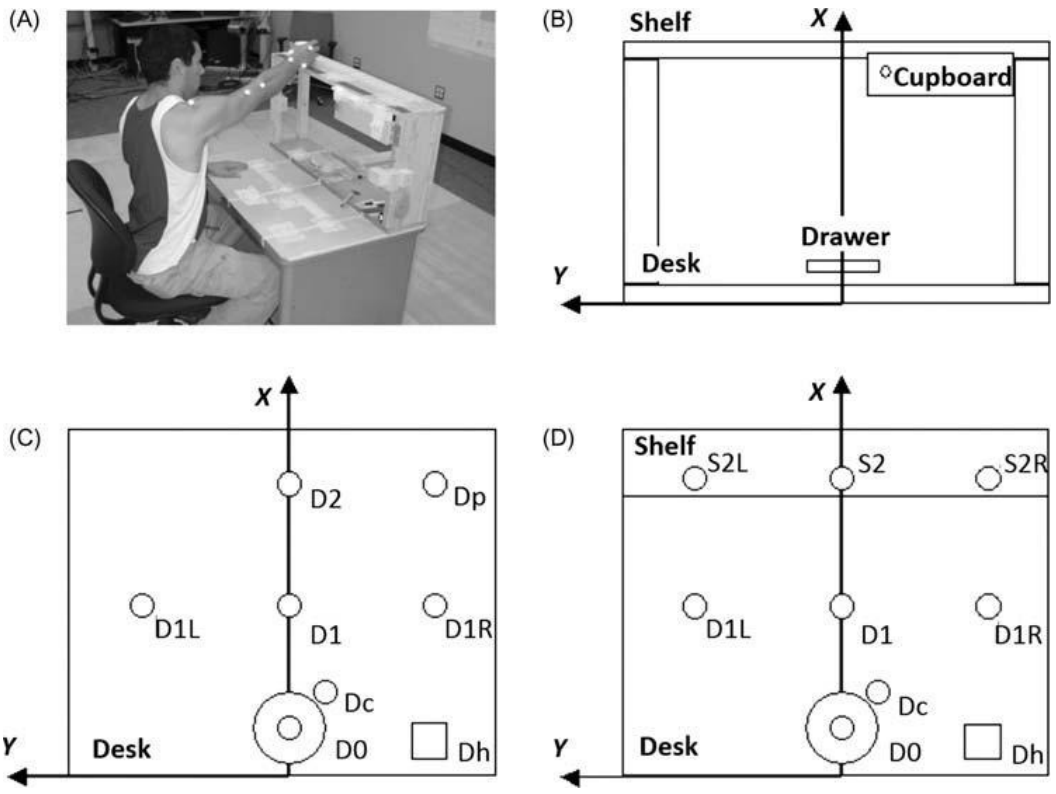

FIGURE 6.5

Desk location from the ADL study. Desk (D) and shelf (S) locations as defined in the ADL study were divided into three medial−lateral, three anterior−posterior, and two superior−inferior positions. Subjects sat in a chair of fixed height for all tasks except opening a door (standing). Reaching actions required moving an object (e.g., a cup) from one location to another and then back (A). A top view of the desktop (C) shows eight target desk locations, more heavily concentrated in the right-hand plane. The three shelf locations were located at the same x-coordinate as desk locations D2 and Dp, only 0.44 m above the desktop in the positive z-direction (D). Also attachable to the desk and shelf were a wood drawer, a cupboard, and a door (B). RP, not shown, refers to the rest pose of the arm lying comfortably along the subject's side.

Reprinted with permission from J.C. Perry, J.M. Powell, J. Rosen, Isotropy of an upper limb exoskeleton and the kinematics and dynamics of the human arm, Appl. Bionics Biomech. 6 (2) (2009) 175–191.

4. Hygiene (actions 20−24): Combing the hair, washing the face, shaving the face, brushing the teeth, and washing the neck.

For more details on the experimental setup and data collection process, readers are encouraged to review the original publication [49].

In the present analysis, only Cartesian position data is used. The ADL dataset provided shoulder positions in terms of Cartesian coordinates with respect to a global origin. For each ADL action, a shoulder origin was established as the mean position of the shoulder in the first 10 motion capture frames. The shoulder displacement for each frame is then taken as the absolute difference of the